Acta Crystallographica Section B
Structural Science
ISSN 0108-7681

Five-coordinate copper(II) complexes: crystal structures, spectroscopic properties and new extended structural pathways of [Cu(chelate)$_2X$]Y, where chelate = dpyam, phen and bipy; X = pseudohalide ligands

Sujittra Youngme,[a]* Pongthipun Phuengphai,[a,b] Chaveng Pakawatchai,[c] Palangpon Kongsaeree[d] and Narongsak Chaichit[e]

[a]Department of Chemistry, Faculty of Science, Khon Kaen University, Khon Kaen 40002, Thailand, [b]Chemistry Program, Faculty of Science and Technology, Surindra Rajabhat University, Surin 32000, Thailand, [c]Department of Chemistry, Faculty of Science, Prince of Songkla University, Hatyai, Songkla 90112, Thailand, [d]Department of Chemistry, Faculty of Science, Mahidol University, Bangkok 10400, Thailand, and [e]Department of Physics, Faculty of Science and Technology, Thammasat University Rangsit, Pathumthani 12121, Thailand

Correspondence e-mail: sujittra@kku.ac.th

Received 8 November 2007
Accepted 11 February 2008

Dedicated to Professor Jan Reedijk on the occasion of his 65th birthday and retirement

The crystal structures of four distortion isomers of the [Cu(chelate)$_2X$]$^+$ cation, where chelate = 2,2-bipyridine (bipy), 1,10-phenanthroline (phen) and di-2-pyridylamine (dpyam), X = a pseudohalide ligand (NCO, NCS, N_3 and C_2N_3), have been compared by scatterplot analysis with 25 [Cu(chelate)$_2X$]Y complexes of known crystal structure. The four new complexes [Cu(phen)$_2$NCO]Br (1), [Cu(phen)$_2N_3$]$BPh_4\cdot H_2O$ (2), [Cu(dpyam)$_2$(N_3)]$NO_3\cdot H_2O$ (3) and [Cu(dpyam)$_2$(N_3)]ClO_4 (4) involve a near regular square-based pyramidal stereochemistry (RSBP). The structures of complexes (1) and (2) are of the rare cases found for the phen analogue. Scatterplots of the 29 cation distortion isomers of the [Cu(chelate)$_2X$]Y series of complexes suggest that most of the 29 complexes lie on a common structural pathway, involving a mixture of the symmetric, C_2, and the asymmetric, non-C_2, in-plane modes of vibration of the CuN_4N' chromophore. Some datapoints are found to lie on extended routes The resulting structural pathways are consistent with the direct observation of the effect of the modes of vibration on the stereochemistries of the complexes. A comparison of the trends in the 29 datasets suggests a size effect of the phen, bipy and dpyam ligands.

1. Introduction

One of the consequences of the Jahn–Teller theorem (Jahn & Teller, 1937; Bersuker, 2001) in the stereochemistry of the copper(II) ion has been termed the plasticity effect (Gazo *et al.*, 1976), which suggests that the various distortion isomers of the copper(II) ion are related by soft modes of vibration of the more regular stereochemistries. Hence the concept of a structural pathway (Nagle *et al.*, 1990; Hathaway, 1984; Burgi & Dunitz, 1983; Dunitz, 1979) for [Cu(chelate)$_2X$]Y-type complexes has been developed (Fig. 1).

In 1984, Addison, Reedijk and co-workers introduced a very useful parameter, τ, which provides a measure of the degree of square-based pyramidal (SBP) *versus* trigonal bipyramidal (TBP) geometry adopted by five-coordinate copper(II) complexes (Addison, Rao, Reedijk *et al.*, 1984). This parameter provides a convenient tool for comparing structures of similar five-coordinate copper(II) complexes. The parameter τ is defined as $(\beta - \alpha)/60$, where β and α are the largest coordination angles, and its value varies from 0 (in regular SBP) to 1 (in regular TBP). The molecular structures of five-coordinate copper(II) complexes range extensively from regular trigonal bipyramidal (RTBP, D_{3h}) to regular square-based pyramidal (RSBP, C_{4v}), see Fig. 2, with most complexes falling between these two stereochemistries (Hathaway & Billing, 1970; Reinen & Friebel, 1984) somewhere along the classical Berry pathway (Addison, Rao & Sinn, 1984). This feature can be useful in probing the relationships between structural correlations and the respective structural pathway involving vibronic-type coupling.

In the majority of $[Cu(chelate)_2X]Y$ complexes the differences in stereochemistry may be associated with the differences in the ligands present, *i.e.* chelate = 2,2-bipyridine (bipy), 1,10-phenanthroline (phen) and di-2-pyridylamine (dpyam), and X = Cl^-, Br^-, I^- or H_2O, respectively. Five-coordinated copper(II) coordination compounds of the general formula $[Cu(dpyam)_2NCO]Y$ (Youngme, Phatchimkun, Suksangpanya *et al.*, 2007) have been previously reported with the limited number of datasets available. Therefore, it is of interest to extend and develop the structural correlations and investigate the existence of a structural pathway (Fig. 3) for the series of five-coordinate copper(II) complexes of the type $[Cu(chelate)_2X]Y$, where chelate = phen, bipy or dpyam, and X is an anion of the pseudohalide ligand (NCO, NCS, N_3 and C_2N_3; Youngme, Phatchimkun, Suksangpanya *et al.*, 2007; Akhter & Hathaway, 1991; McAuliffe *et al.*, 1992; Munno *et al.*, 1998; Potočňák *et al.*, 1995, 1996*a*,*b*, 1998*a*,*b*, 2001, 2002, 2003, 2005). In Fig. 3 the new extended structural pathways and distortion of α_8 (N1—Cu—N3) are presented and investigated. To obtain this extended database of 29 complexes, the crystal structures of four new compounds, $[Cu(phen)_2NCO]Br$ (1), $[Cu(phen)_2N_3]BPh_4{\cdot}H_2O$ (2), $[Cu(dpyam)_2(N_3)]NO_3{\cdot}H_2O$ (3) and $[Cu(dpyam)_2(N_3)]ClO_4$ (4), have been determined and are now reported.

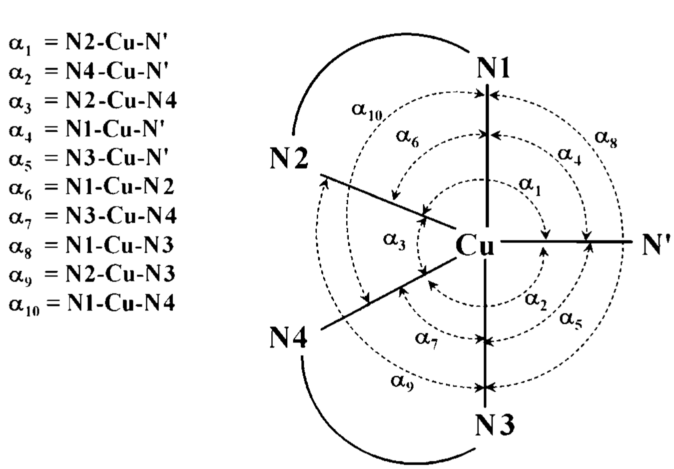

Figure 1
The atom-numbering scheme and α_n notation for the CuN_4N' chromophore.

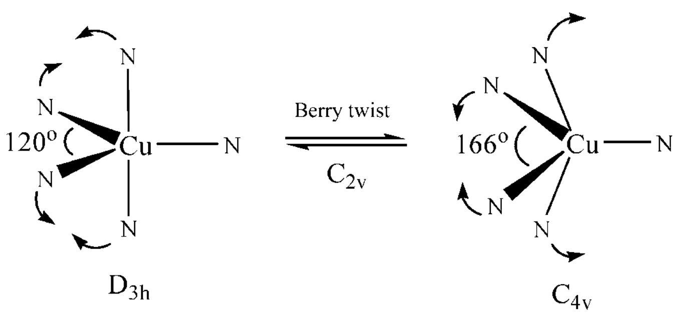

Figure 2
The Berry twist mechanism for interconversion of a regular trigonal bypyramid to square pyramid.

2. Experimental

All reagents were commercial-grade and were used without further purification. Elemental analyses (C, H and N) were performed on a Perkin–Elmer PE2400 CHNS/O analyzer. The IR spectra were recorded on a Spectrum One Perkin–Elmer FT-IR spectrophotometer as KBr pellets in the 4000–450 cm^{-1} region. Solid-state (diffuse reflectance) electronic spectra were recorded as polycrystalline samples on a Perkin–Elmer Lambda2S spectrophotometer over the range 8000–18 000 cm^{-1}.

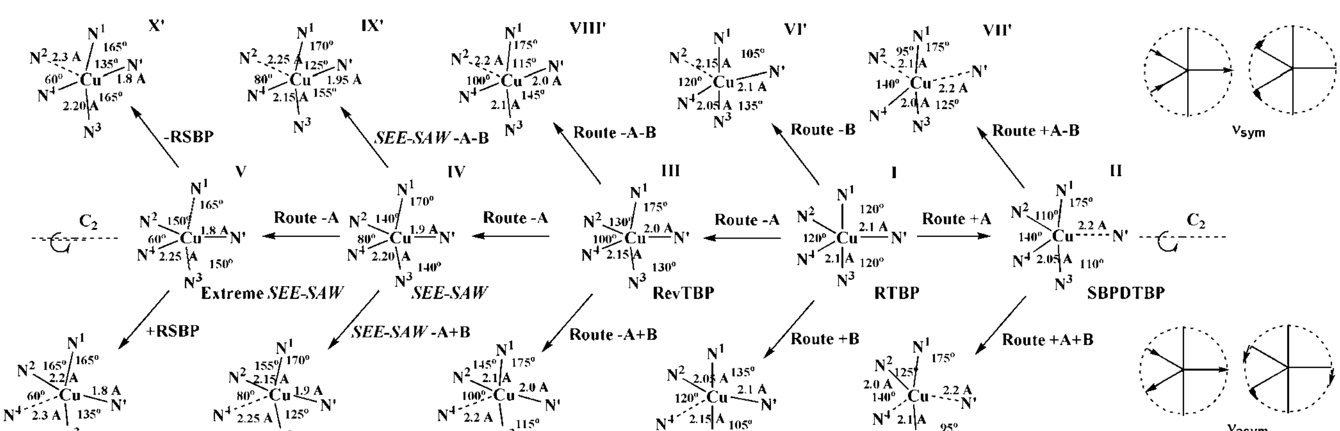

Figure 3
The forms of distortion of the RTBP CuN_4N' chromophore involving the $\pm A$, $\pm B$ and $\pm A$ $\pm B$ routes.

Table 1
Crystal and refinement data for (1)–(4).

	(1)	(2)	(3)	(4)
Crystal data				
Chemical formula	$C_{25}H_{16}BrCuN_5O$	$C_{48}H_{36}BCuN_7O$	$C_{20}H_{20}CuN_{10}O_4$	$C_{20}H_{18}ClCuN_9O_4$
M_r	545.88	801.19	528.00	547.42
Cell setting, space group	Triclinic, $P\bar{1}$	Triclinic, $P\bar{1}$	Triclinic, $P\bar{1}$	Monoclinic, $P2_1/c$
Temperature (K)	293 (2)	293 (2)	293 (2)	293 (2)
a, b, c (Å)	8.9141 (18), 10.448 (2), 12.291 (3)	10.2373 (4), 11.3628 (4), 19.1037 (7)	7.7515 (6), 9.9160 (8), 15.2750 (12)	13.4360 (5), 8.3880 (3), 22.5750 (5)
α, β, γ (°)	78.688 (4), 81.562 (4), 72.798 (3)	86.6970 (10), 75.8840 (10), 67.7440 (10)	100.0100 (10), 103.3470 (10), 99.5270 (10)	90.00, 118.1471 (19), 90.00
V (Å^3)	1067.4 (4)	1993.07 (13)	1098.78 (15)	2243.35 (13)
Z	2	2	2	4
D_x (Mg m^{-3})	1.698	1.335	0.798	1.621
Radiation type	Mo $K\alpha$	Mo $K\alpha$	Mo $K\alpha$	Mo $K\alpha$
μ (mm^{-1})	2.92	0.60	0.52	1.14
Crystal form, colour	Prismatic, green	Prismatic, blue	Prismatic, blue–green	Prismatic, blue–green
Crystal size (mm)	0.19 × 0.09 × 0.03	0.38 × 0.20 × 0.10	0.24 × 0.18 × 0.10	0.15 × 0.12 × 0.05
Data collection				
Diffractometer	Bruker SMART CCD	Bruker SMART CCD	Bruker SMART CCD	Bruker SMART CCD
Data collection method	ω scans	ω scans	ω scans	ω scans
Absorption correction	Semi-emperical *SADABS*	Semi-emperical *SADABS*	Semi-emperical *SADABS*	Semi-emperical *SADABS*
T_{min}	0.657	0.689	0.842	0.657
T_{max}	1.000	1.000	1.000	1.000
No. of measured, independent and observed reflections	10 680, 3901, 3161	10 733, 7178, 4805	12 952, 5157, 4510	19 249, 4240, 3248
Criterion for observed reflections	$I > 2\sigma(I)$	$I > 2\sigma(I)$	$I > 2\sigma(I)$	$I > 2\sigma(I)$
R_{int}	0.030	0.033	0.021	0.058
θ_{max} (°)	25.4	25.4	28.3	25.8
Refinement				
Refinement on	F^2	F^2	F^2	F^2
$R[F^2 > 2\sigma(F^2)]$, $wR(F^2)$, S	0.039, 0.093, 1.04	0.069, 0.182, 1.13	0.036, 0.092, 1.04	0.045, 0.125, 1.03
No. of reflections	3901	7178	5157	4240
No. of parameters	298	532	423	417
H-atom treatment	Mixture of independent and constrained refinement	Mixture of independent and constrained refinement	Mixture of independent and constrained refinement	Mixture of independent and constrained refinement
Weighting scheme	$w = 1/[\sigma^2(F_o^2) + (0.0476P)^2 + 0.2281P]$, where $P = (F_o^2 + 2F_c^2)/3$	$w = 1/[\sigma^2(F_o^2) + (0.0671P)^2 + 1.4556P]$, where $P = (F_o^2 + 2F_c^2)/3$	$w = 1/[\sigma^2(F_o^2) + (0.0507P)^2 + 0.2291P]$, where $P = (F_o^2 + 2F_c^2)/3$	$w = 1/[\sigma^2(F_o^2) + (0.066P)^2 + 1.310P]$, where $P = (F_o^2 + 2F_c^2)/3$
$(\Delta/\sigma)_{max}$	0.005	0.005	0.013	0.042
$\Delta\rho_{max}$, $\Delta\rho_{min}$ (e Å^{-3})	0.41, −0.29	0.42, −0.48	0.32, −0.24	0.40, −0.48

Computer programs used: *SMART* (Bruker, 2001*b*), *SAINT* (Bruker, 2001*a*), *SHELXS*97, *SHELXL*97 (Sheldrick, 2008), *SHELXTL* (Bruker, 2000).

2.1. Preparation of (1)–(4)

[Cu(phen)$_2$NCO]Br (1): A warm solution of phen (0.198 g, 1.0 mmol) in methanol (15 cm^3) was added to a hot aqueous solution (15 cm^3) of $CuBr_2$ (0.112 g, 0.5 mmol). An aqueous solution (10 cm^3) of KNCO (0.081 g, 1.0 mmol) was then added to the reaction mixture. The green solution was slowly evaporated at room temperature. Green crystals of (1) deposited after several days. The crystals were filtered off, washed with mother liquor and air-dried. Yield *ca* 65%. Analysis: calc. for $C_{25}H_{16}BrCuN_5O$ (%): C 55.00, H 2.95, N 12.83; found: C 55.08, H 3.02, N 13.07.

[Cu(phen)$_2$N$_3$]BPh$_4$·H$_2$O (2): A warm solution of phen (0.198 g, 1.0 mmol) in methanol (15 cm^3) was added to a hot aqueous solution (15 cm^3) of Cu(O$_2$CCH$_3$)$_2$·H$_2$O (0.091 g, 0.5 mmol). An aqueous solution (10 cm^3) of NaN_3 (0.065 g, 1.0 mmol) was then added to the reaction mixture. Then solid $NaBPh_4$ (0.171 g, 0.5 mmol) was added and the reaction mixture was stirred continuously. The green solution was slowly evaporated at room temperature. Green crystals of (2) deposited after several days. The crystals were filtered off, washed with mother liquor and air-dried. Yield *ca* 80%. Analysis: calc. for $C_{48}H_{36}BCuN_7O$ (%): C 71.95, H 4.52, N 12.23; found: C 72.07, H 4.39, N 12.31.

[Cu(dpyam)$_2$N$_3$]NO$_3$·H$_2$O (3): A warm solution of dpyam (0.171 g, 1.0 mmol) in methanol (15 cm^3) was added to a hot aqueous solution (15 cm^3) of Cu(NO$_3$)$_2$·3H$_2$O (0.121 g, 0.5 mmol). An aqueous solution (10 cm^3) of NaN_3 (0.065 g, 1.0 mmol) was then added to the reaction mixture. The green solution was slowly evaporated at room temperature. Dark green crystals of (3) deposited after several days. The crystals were filtered off, washed with mother liquor and air-dried. Yield *ca* 75%. Analysis: calc. for $C_{20}H_{20}CuN_{10}O_4$ (%): C 45.50, H 3.82, N 26.52; found: C 45.63, H 3.76, N 26.51.

[Cu(dpyam)$_2$N$_3$]ClO$_4$ (4): A warm solution of dpyam (0.171 g, 1.0 mmol) in methanol (15 cm^3) was added to a hot

Table 2
Selected bond lengths (Å) and angles (°) for $[Cu(L)_2(X)]Y$.

L = dpyam										L = phen	L = bipy	
Y =	Br^-	$CF_3SO_3^-$	BF_4^-·dpyam	Cl^-·$4H_2O$	NO_3^-	$(SO_4)^{2-}_{0.5}$·-dpyam·$0.5H_2O$	PF_6^-	ClO_4^-	BPh_4^-	Br^-	ClO_4^-	$C(CN)_3^-$
	(5)[a]	(6)[a]	(7)[a]	(8)[a]	(9)[a]	(10)[b]	(11)[a]	(12)[a]	(13)[a]	(1)[c]	(19)[d]	(20)[e]
(a) X = NCO												
Cu—N′	1.945 (3)	1.949 (3)	1.933 (4)	1.955 (5)	1.950 (3)	1.903 (13)	1.949 (3)	1.952 (4)	1.984 (1)	1.948 (3)	1.961 (8)	1.949 (4)
Cu—N1	2.030 (3)	2.029 (3)	2.000 (4)	2.008 (3)	2.008 (2)	2.028 (10)	2.008 (2)	2.002 (3)	2.017 (1)	2.029 (3)	2.007 (9)	1.983 (3)
Cu—N3	2.045 (3)	2.025 (3)	2.001 (3)	2.012 (3)	2.008 (3)	2.012 (10)	2.013 (2)	2.013 (3)	2.018 (1)	2.047 (3)	1.981 (8)	2.003 (3)
Cu—N2	2.021 (3)	2.047 (2)	2.025 (3)	2.016 (4)	2.043 (2)	2.014 (10)	2.074 (2)	2.068 (3)	2.072 (1)	2.039 (3)	2.095 (8)	2.054 (3)
Cu—N4	2.283 (3)	2.245 (3)	2.157 (4)	2.181 (3)	2.185 (2)	2.162 (10)	2.169 (3)	2.167 (3)	2.089 (1)	2.345 (3)	2.111 (7)	2.158 (3)
α_1	167.1 (1)	159.4 (1)	156.2 (1)	157.9 (1)	157.3 (1)	154.7 (5)	144.6 (1)	144.1 (2)	124.7 (2)	170.9 (1)	133.2 (1)	141.7 (2)
α_2	98.8 (2)	102.8 (2)	104.4 (1)	104.0 (1)	109.1 (1)	104.6 (5)	116.9 (1)	115.6 (1)	119.4 (1)	100.2 (1)	121.6 (1)	114.5 (1)
α_3	94.1 (2)	97.8 (1)	99.3 (1)	98.1 (1)	93.7 (1)	100.7 (5)	98.5 (1)	100.2 (1)	115.9 (1)	87.6 (1)	105.2 (1)	103.8 (1)
α_4	92.7 (1)	94.2 (2)	90.4 (1)	89.4 (1)	92.5 (1)	90.1 (5)	89.6 (1)	89.6 (1)	94.9 (1)	94.5 (1)	93.4 (1)	95.1 (1)
α_5	92.4 (1)	92.4 (1)	87.8 (1)	88.3 (1)	91.8 (1)	90.0 (5)	88.0 (2)	87.4 (1)	94.7 (1)	93.6 (1)	92.5 (1)	93.0 (1)
α_6	86.2 (1)	86.2 (1)	87.5 (1)	86.6 (1)	86.4 (1)	85.5 (4)	87.7 (1)	88.3 (1)	89.1 (1)	80.8 (1)	79.5 (1)	80.2 (1)
α_7	82.2 (1)	85.3 (1)	88.7 (1)	86.0 (1)	86.1 (1)	85.9 (5)	87.2 (2)	87.7 (1)	88.5 (1)	76.3 (1)	79.5 (1)	78.3 (1)
α_8	172.8 (1)	173.1 (1)	170.0 (2)	173.7 (1)	175.3 (1)	173.0 (5)	176.2 (1)	176.2 (1)	170.3 (2)	164.9 (1)	173.7 (1)	171.6 (1)
α_9	89.9 (1)	88.3 (1)	90.2 (1)	93.3 (1)	88.9 (1)	91.5 (4)	92.6 (1)	92.7 (1)	86.2 (1)	92.8 (1)	94.8 (1)	94.8 (1)
α_{10}	92.0 (1)	91.3 (1)	101.3 (1)	100.3 (1)	94.2 (1)	100.9 (5)	96.5 (1)	95.7 (1)	85.9 (1)	89.7 (1)	99.3 (1)	96.3 (1)
τ	0.09	0.23	0.23	0.26	0.30	0.31	0.53	0.54	0.76	0.10	0.68	0.50

L = dpyam					L = phen	L = bipy
Y =	NO_3^-·H_2O (3)[c]	ClO_4^- (4)[c]	PF_6^- (14)[f]	Cl^-·$4H_2O$ (15)[f]	BPh_4^-·H_2O (2)[c]	ClO_4^- (23)[g]
(b) X = N_3						
Cu—N′	2.020 (1)	2.016 (3)	2.009 (2)	2.007 (2)	1.980 (4)	1.971 (5)
Cu—N1	2.001 (1)	1.995 (3)	2.005 (2)	1.999 (2)	2.006 (4)	2.001 (4)
Cu—N3	2.016 (1)	2.027 (3)	2.036 (2)	2.003 (2)	2.022 (4)	2.019 (4)
Cu—N2	2.022 (1)	2.017 (3)	2.016 (2)	2.028 (2)	2.045 (4)	2.030 (5)
Cu—N4	2.158 (1)	2.165 (3)	2.153 (2)	2.169 (2)	2.242 (4)	2.218 (5)
α_1	160.5 (1)	168.2 (1)	166.8 (1)	160.5 (1)	166.7 (1)	164.4 (2)
α_2	98.8 (1)	95.2 (1)	96.5 (1)	103.4 (1)	100.6 (1)	105.4 (2)
α_3	100.7 (1)	96.6 (1)	96.7 (1)	96.0 (1)	92.2 (1)	90.0 (2)
α_4	89.1 (1)	88.7 (1)	88.2 (1)	86.4 (1)	90.3 (1)	92.2 (2)
α_5	88.5 (1)	89.6 (1)	90.2 (1)	89.0 (1)	91.5 (1)	89.2 (2)
α_6	87.0 (1)	88.5 (1)	88.0 (1)	87.4 (1)	81.4 (1)	80.5 (2)
α_7	88.0 (1)	89.5 (1)	88.8 (1)	87.9 (1)	78.2 (1)	77.7 (2)
α_8	165.8 (1)	161.7 (1)	163.1 (1)	169.4 (1)	170.4 (1)	173.3 (1)
α_9	90.8 (1)	89.5 (1)	89.8 (1)	93.9 (1)	94.9 (1)	96.6 (2)
α_{10}	106.2 (1)	108.9 (1)	108.2 (1)	102.5 (1)	110.8 (1)	108.2 (2)
τ	0.09	0.11	0.06	0.15	0.06	0.15

L = bipy		L = dpyam	L = phen			L = phen				L = bipy	
Y =	$C(CN)_3^-$ (22)[h]	NCS·0.5DMSO (16)[i]	$ONC(CN)_2^-$ (21)[j]	ClO_4^- (17)[k]	$C(CN)_3^-$ (18)[l]	ClO_4^- (24)[m]	$CF_3SO_3^-$ (25)[n]	$C(CN)_3^-$ (26)[o]	PF_6^- (27)[p]	ClO_4^- (28)[q]	BF_4^- (29)[r]
(c) X = NCS						(d) X = C_2N_3					
Cu—N′	1.978 (4)	1.976 (4)	1.963 (3)	2.005 (5)	1.984 (4)	2.033 (6)	1.990 (2)	1.982 (4)	1.983 (3)	1.995 (3)	2.015 (3)
Cu—N1	1.970 (3)	1.997 (3)	1.980 (3)	2.004 (4)	1.987 (3)	1.996 (5)	1.995 (2)	1.977 (4)	2.003 (3)	1.992 (1)	1.998 (3)
Cu—N3	1.979 (3)	2.017 (3)	1.994 (3)	1.999 (4)	2.000 (3)	2.001 (5)	1.990 (2)	1.981 (3)	1.986 (3)	2.003 (1)	2.006 (3)
Cu—N2	2.064 (3)	2.017 (3)	2.080 (3)	2.089 (4)	2.078 (3)	2.086 (4)	2.108 (2)	2.064 (3)	2.100 (3)	2.040 (1)	2.043 (3)
Cu—N4	2.094 (3)	2.164 (3)	2.101 (3)	2.113 (4)	2.112 (3)	2.087 (5)	2.141 (2)	2.112 (4)	2.122 (3)	2.146 (1)	2.142 (3)
α_1	126.3 (1)	158.6 (1)	128.0 (1)	126.0 (1)	126.6 (1)	118.4 (1)	135.3 (1)	133.6 (2)	133.3 (1)	146.7 (1)	145.0 (1)
α_2	117.9 (1)	103.9 (1)	115.8 (1)	118.0 (2)	113.2 (1)	115.2 (1)	121.2 (1)	115.7 (2)	122.4 (1)	108.5 (1)	108.6 (1)
α_3	115.8 (1)	97.4 (1)	116.2 (1)	116.1 (1)	120.2 (1)	126.4 (2)	103.5 (1)	110.7 (1)	104.3 (1)	104.9 (1)	106.4 (1)
α_4	93.1 (1)	88.9 (1)	93.6 (1)	92.8 (2)	92.8 (1)	90.4 (2)	91.9 (1)	93.4 (2)	90.6 (1)	92.5 (1)	92.4 (1)
α_5	92.6 (1)	88.1 (1)	93.9 (1)	92.2 (2)	93.2 (1)	90.4 (2)	93.1 (1)	91.4 (2)	93.7 (1)	90.3 (1)	90.0 (1)
α_6	80.0 (1)	87.4 (1)	80.9 (1)	80.6 (2)	80.8 (1)	80.8 (2)	81.1 (1)	80.8 (1)	80.8 (1)	80.5 (1)	80.5 (1)
α_7	79.6 (1)	89.0 (1)	80.5 (1)	80.4 (2)	80.5 (1)	80.7 (1)	80.4 (1)	80.7 (1)	80.6 (1)	78.8 (1)	79.1 (1)
α_8	174.2 (1)	166.2 (1)	172.3 (1)	174.8 (2)	174.0 (1)	179.1 (2)	175.0 (1)	175.1 (1)	175.3 (1)	177.2 (1)	177.5 (1)
α_9	97.5 (1)	90.5 (1)	95.9 (1)	97.6 (1)	96.6 (1)	98.6 (2)	95.1 (1)	95.2 (1)	94.8 (1)	96.9 (1)	97.2 (1)
α_{10}	96.7 (1)	104.9 (1)	94.6 (1)	95.9 (2)	96.0 (1)	99.0 (1)	97.2 (1)	98.0 (1)	98.7 (1)	100.8 (1)	100.8 (1)

Table 2 (continued)

L = bipy		L = dpyam	L = phen			L = phen				L = bipy	
Y =	$C(CN)_3^-$ (22)[h]	NCS·0.5DMSO (16)[i]	$ONC(CN)_2^-$ (21)[j]	ClO_4^- (17)[k]	$C(CN)_3^-$ (18)[l]	ClO_4^- (24)[m]	$CF_3SO_3^-$ (25)[n]	$C(CN)_3^-$ (26)[o]	PF_6^- (27)[p]	ClO_4^- (28)[q]	BF_4^- (29)[r]
τ	0.80	0.13	0.74	0.81	0.79	0.88	0.66	0.69	0.70	0.51	0.54

References: (*a*) Youngme, Phatchimkun, Suksangpanya *et al.* (2007), (*b*) Akhter & Hathaway (1991), (*c*) this work, (*d*) McAuliffe *et al.* (1992), (*e*) Potočňák *et al.* (1998*a*), (*f*) Youngme, Phatchimkun, Pakawatchai *et al.*, 2007), (*g*) Munno *et al.* (1998), (*h*) Potočňák *et al.* (1998*b*), (*i*) Youngme *et al.* (2002), (*j*) Potočňák *et al.* (1995), (*k*) Parker *et al.* (1994), (*l*) Potočňák *et al.* (1996*a*), (*m*) Burčák *et al.* (2004), (*n*) Potočňák *et al.* (2003), (*o*) Potočňák *et al.* (1996*b*), (*p*) Potocnák *et al.* (2005), (*q*) Potočňák *et al.* (2002), (*r*) Potočňák *et al.* (2001).

aqueous solution (15 cm^3) of $Cu(ClO_4)_2{\cdot}4H_2O$ (0.185 g, 0.5 mmol). An aqueous solution (10 cm^3) of NaN_3 (0.065 g, 1.0 mmol) was then added to the reaction mixture. The green solution was slowly evaporated at room temperature. Green crystals of (4) deposited after several days. The crystals were filtered off, washed with mother liquor and air-dried. Yield *ca* 90%. Analysis: calc. for $C_{20}H_{18}ClCuN_9O_4$ (%): C 43.88, H 3.31, N 23.03; found: C 43.96, H 3.23, N 23.11.

2.2. Crystallography

Reflection data for (1)–(4) were collected at 293 K on a 4 K Bruker SMART CCD area-detector diffractometer using graphite-monochromated Mo $K\alpha$ radiation (λ = 0.71073 Å) at a detector distance of 6.0 cm and swing angle of -28°. A hemisphere of the reciprocal space was covered by a combination of three sets of exposures; each set had a different φ angle (0, 88, 180°) and each exposure of 10 s for (1)–(4) covered 0.3° in ω. Data reduction and cell refinements were performed using the program *SAINT* (Siemens, 1996). An empirical absorption correction was applied using the *SADABS* (Sheldrick, 1996) program. The structure was solved by direct methods and refined by the full-matrix least-squares method on $(F_{obs})^2$ with anisotropic displacement parameters for all non-H atoms using the *SHELXTL-PC* (Siemens, 1997) software package.

The NO_3^- anion in (3) and ClO_4^- anion in (4) are disordered with site occupancies of 0.50 for both conformers. The molecular graphics were created using *SHELXTL-PC*. The crystal and refinement details for (1)–(4) are listed in Table 1.[1] Selected bond lengths and angles are given in Table 2.

3. Results and discussion

3.1. Crystal structures

Fig. 1 shows a representative molecular structure for the $[Cu(chelate)_2X]$ cation, with atom numbering and the angular notation schemes used. The crystallographic and refinement data for the four new complexes reported are given in Table 1. Table 2(*a*) reports the Cu—L distances and α_{1-10} angles of the 12 $[Cu(chelate)_2NCO]Y$ complexes (1), (5)–(13) and (19)–(20). Table 2(*b*) lists the corresponding data for the six $[Cu(chelate)_2N_3]^+$ cations (2)–(4), (14)–(15) and (23). Table 2(*c*) lists the data for the five $[Cu(chelate)_2NCS]^+$ cations (16)–(18), (21) and (22), and Table 2(*d*) lists the data for the six $[Cu(chelate)_2C_2N_3]^+$ cations (24)–(29), thus extending the database to 29 $[Cu(chelate)_2(X)]^+$ cations. The corresponding τ values, where $\tau = (\alpha_8 - \alpha_1)/60$ (Addison, Rao, Reedijk *et al.*, 1984), are listed, with τ = 1.00 for an RTBP and τ = 0.00 for an RSBP. Table 3 reports the maximum and minimum values of the Cu—L distances and α_n angles, their differences and average values. In Table 2, the axial positions, N1 and N3, are defined as the largest N—Cu—N angle of *ca* 180°, usually $\alpha_8 > \alpha_1$ except complexes (1), (4) and (14). The longest in-plane distance, Cu—N4, is defined as opposite the largest in-plane angle α_1, with $\alpha_1 > \alpha_2 > \alpha_3$, except the complexes (3), (4), (14), (18), (21) and (24), $\alpha_2 < \alpha_3$. These are due to the flexibility of the molecular structures. The Cu—N′ distances observed appear to be shorter than the in-plane Cu—N2,4 distances. The results for the new structures will not be compared in detail, but compared with earlier data by scatterplot analysis.

3.2. The $[Cu(chelate)_2X]Y$ data

For the 29 $[Cu(chelate)_2X]Y$ complexes, where chelate = phen, bipy or dpyam and X is an anion of a pseudohalide ligand (NCO, NCS, N_3 and C_2N_3; Table 2), the structure of the five-coordinate CuN_4N' chromophore varies from square-based pyramidal distorted trigonal bipyramidal, SBPDTBP, for (24) (τ = 0.88) to the near RSBP for (2) (τ = 0.06) and $\Delta\tau$ = 0.82. This is a large variation in τ, the largest seen to date for the cation distortion isomers of the $[Cu(chelate)_2X]Y$ series of complexes (Camus *et al.*, 1999; Johnson & Jacobson, 1973; Jensen & Jacobson, 1981). None of the complexes have a near RTBP (regular trigonal bipyramidal) stereochemistry or lies on a twofold axis of symmetry. There are 14 complexes [(1)–(10), (14)–(16) and (23)] which have τ values in the more limited range 0.06–0.31 and their stereochemistries are best described as TBPDSBP. Five complexes [(11)–(12), (20) and (28)–(29)] have τ values of 0.50–0.54 and their stereochemistries are best described as intermediate five-coordinate. Ten complexes [(13), (17)–(19), (21)–(22), (24)–(27)] have τ values in the range 0.66–0.88 and their stereochemistries are best described as SBPDTBP. Table 3 reports the maximum and minimum values of the Cu—L distances and α_n angles, their differences and average values for $[Cu(chelate)_2X]Y$ complexes. Relative to a RTBP stereochemistry, the out-of-plane distances (Table 2) show only small differences (Table 3)

[1] Supplementary data for this paper are available from the IUCr electronic archives (Reference: BP5008). Services for accessing these data are described at the back of the journal.

Table 3
Maxima, minima, difference (Δ) and average values of the bond lengths (Å) and angles (°) for the $[Cu(chelate)_2X]Y$ complexes.

	Out-of-plane bond lengths		In-plane bond lengths			
	Cu—N1	Cu—N3	Cu—N′	Cu—N2	Cu—N4	τ
Maximum	2.030 (1)	2.047 (1)	2.033 (6)	2.108 (2)	2.345 (3)	0.88
Minimum	1.970 (1)	1.979 (1)	1.903 (13)	2.014 (10)	2.087 (5)	0.06
Δ	0.060	0.068	0.130	0.094	0.258	0.82
Average	1.998 (1)	2.006 (1)	1.975 (1)	2.052 (1)	2.162 (1)	

	In-plane angles			Out-of -plane angles						
	α_1	α_2	α_3	α_4	α_5	α_6	α_7	α_8	α_9	α_{10}
Maximum	170.9 (1)	122.4 (1)	126.4 (1)	95.1 (1)	94.7 (1)	89.1 (1)	89.5 (1)	179.1 (1)	98.6 (1)	110.8 (1)
Minimum	118.4 (1)	95.2 (1)	87.6 (1)	86.4 (1)	87.4 (1)	79.5 (1)	76.3 (1)	161.7 (2)	86.2 (1)	85.9 (1)
Δ	52.5	27.2	38.8	8.7	7.3	9.6	13.2	17.4	12.4	24.9
Average	147.5 (1)	109.4 (1)	103.1 (1)	91.5 (1)	91.0 (2)	83.8 (1)	83.2 (1)	172.2 (1)	93.4 (1)	99.0 (1)

with ΔCu—N1 = 0.060 Å and ΔCu—N3 = 0.068 Å. The largest variations in bond lengths are present in the equatorial bond distances Cu—N4, Cu—N′ and Cu—N2, respectively. The Cu—N4 distances show the largest variation ranging from 2.087 (5) to 2.345 (3) Å, with Δ = 0.258 Å and with an average value of 2.162 (1) Å. The Cu—N2 distances vary from 2.014 (10) to 2.108 (2) Å, with Δ = 0.094 Å and with a mean value of 2.052 (1) Å. The Cu—N′ distances range from 1.903 (13) to 2.033 (6) Å, with Δ = 0.130 Å and with an average value of 1.975 (1) Å. The average of the in-plane Cu—N(2, 4, N′) distances, 2.063 (1) Å, is greater than the average of the axial Cu—N(1,3) distances [2.005 (1) Å], by 0.058 Å, consistent with a TBP stereochemistry and slightly less than the difference of 0.1 Å normally observed (Huq & Shapski, 1971). The out-of-plane bond angles (Table 2) show only small differences, Table 3, with $\Delta\alpha_{4-7}$ and $\Delta\alpha_{8-10}$ ranging from 7.3 to 13.2 and 12.4 to 24.9°, respectively. The α_1 in-plane angles show the largest variation ranging from 118.4 (1) to 170.9 (1)°, with Δ = 52.5° and with a mean value of 147.5 (1)°. The α_2 angles show the smallest variation ranging from 95.2 (1) to 122.4 (1)°, with Δ = 27.2° and an average value of 109.4 (1)°. The α_3 angles vary from 87.6 (1) to 126.4 (1)°, with Δ = 38.8° and an average value of 103.1 (1)°. From Table 2 it is noticeable that within the τ value range of 0.88–0.06 there is a slight gap of 0.04 between the value of 0.70 for (27) to the next value of 0.74 for (21). This gap corresponds to a change in the ratio of the α_9 and α_{10} angles, for τ values > 0.70, $\alpha_9 > \alpha_{10}$, but for τ values < 0.70, $\alpha_9 < \alpha_{10}$. These relations have been used to suggest a structural pathway from regular trigonal bipyramidal to distorted square-based pyramidal and suggest that (1)–(29) lie in a more extensive structural pathway for the CuN_4N' chromophore.

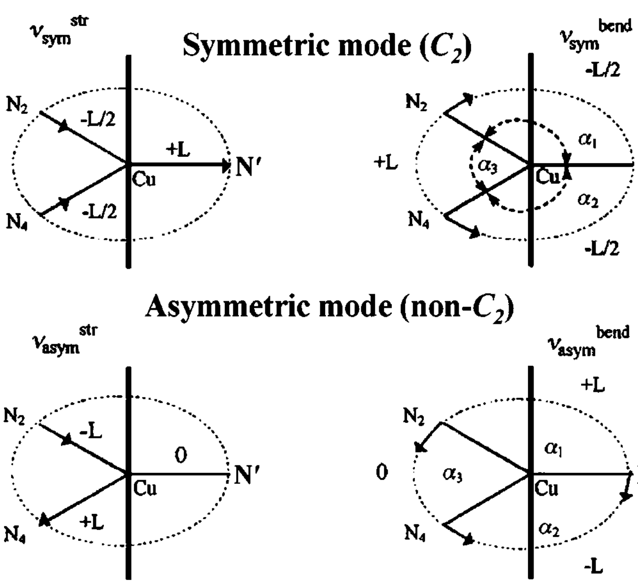

Figure 4
The symmetric and asymmetric modes of vibration for the five-coordinate CuN_4N' chromophore, including the relative magnitudes (L).

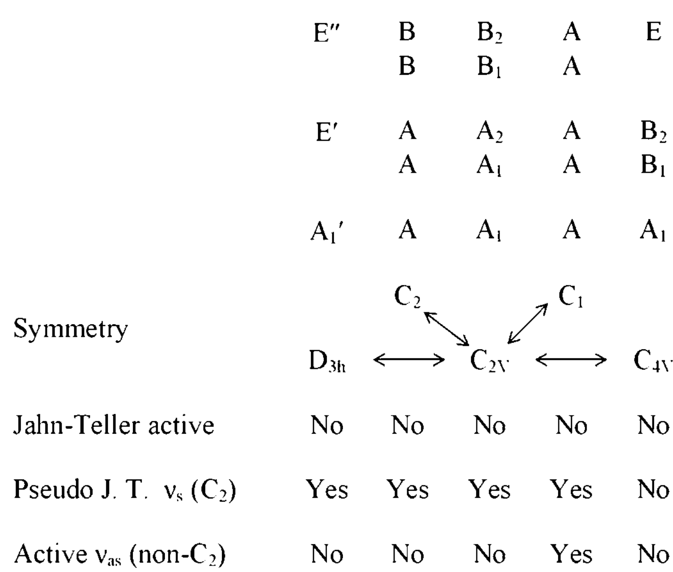

Figure 5
The one-electron orbital levels of the RTBP stereochemistry and their symmetries in various point groups.

Table 4
Limiting values for $\pm A$, $+B$, $-A + B$ and $+A + B$ route distortions.

	RTBP	$+A$ (RSBP)	$-A$ (SEESAW)	$+B$	$-B$	$-A + B$ (SBP)	$+A + B$ (SBP)
α_1 (°)	120	97.5	135	150	90	165	105
α_2 (°)	120	97.5	135	90	150	105	90
α_3 (°)	120	165	90	120	120	90	165
Cu—N4 (Å)	2.092	1.998	2.155	2.199	1.985	2.262	2.025
Cu—N2 (Å)	2.092	1.998	2.155	1.985	2.199	2.048	1.971
Cu—N′ (Å)	2.092	2.280	1.966	2.092	2.092	1.966	2.280

3.3. Interpretation of the $\pm A$ and $\pm B$ route distortions in terms of modes of vibration

In the distortion of RTBP to RSBP stereochemistry the modes of vibration of the in-plane CuN_2N' portion of the chromophore involved are ν^{str}_{sym}, ν^{bend}_{sym}, ν^{str}_{asym} and ν^{bend}_{asym} (Fig. 4). These senses of distortion can be conveniently described in terms of the $\pm A$ and $\pm B$ routes of Fig. 5. The $\pm A$ route of distortion involves solely ν^{str}_{sym} and ν^{bend}_{sym} modes of vibration, both of which retain the C_2 symmetry of the CuN_4N' chromophore. On the other hand, the $\pm B$ route of distortion is determined by the ν^{str}_{asym} and ν^{bend}_{asym} modes, both of which lower the symmetry of the CuN_4N' chromophore to C_1. In practice, the CuN_4N' chromophores display no elements of symmetry, *i.e.* they have C_1 symmetry (Table 2 and Fig. 5). Thus, the $[Cu(chelate)_2X]Y$ series of complexes are described with $-A$ route distortion, which also involves a significant $+B$ route distortion. The pure $-A$ route distortion with C_2 symmetry is represented by the left horizontal distortion through the RTBP stereochemistry in Fig. 5, as a *reversed* trigonal bipyramidal (RevTBP) stereochemistry, implying that the pure $+A$ route distortion (illustrated by the right horizontal distortion in Fig. 5) is referred to as SBPDTBP. However, as the actual datapoints rarely involve pure $\pm A$ or $\pm B$ route distortions, all four modes are generally involved in the distortion of each complex. As the α_3 angles are nearly 40° less than the 120° of the RTBP stereochemistry, it is inappropriate to describe them as RevTBP and so the term *SEESAW* distorted trigonal bipyrimidal (SSDTBP) has been introduced to describe their geometries; however, it should be noted that the distinction between these two geometries is only arbitrary.

3.4. Scatterplot analysis for the [Cu(chelate)$_2$*X*]*Y* series of complexes

This section presents the data for the $[Cu(chelate)_2X]Y$ series of complexes (Table 2) using scatterplot analysis. The scatterplots (Figs. 6–12) discussed are as follows: τ *versus* Cu—N4 (Fig. 6), α_1 *versus* α_3 (Fig. 7), Cu—N2 *versus* Cu—N4 (Fig. 8), α_2, α_1 *versus* α_3 (Fig. 9), Cu—N′ *versus* Cu—N4 (Fig. 10), Cu—N4 *versus* Cu—N′ (Fig. 11*a*), Cu—N4 *versus* Cu—N2 (Fig. 11*b*) and α_3 *versus* Cu—N′ (Fig. 12). A general discussion on the use of scatterplots has been previously reported (Youngme, Phatchimkun, Suksangpanya *et al.*, 2007) and will now be applied to the 29 $[Cu(chelate)_2X]^+$ cations. Using the suggested limiting values (Table 4) for the $\pm A$, $\pm B$ and $\pm A \pm B$ route distortions illustrated in Fig. 5, the angle *versus* angle plots and distance *versus* distance plots can be divided to represent $\pm A$, $\pm B$ axes and $\pm A \pm B$ sections (Figs. 6–12).

An overview of the range of stereochemistries is provided by the plot of τ *versus* Cu—N4 in Fig. 6. However, as τ involves two simultaneous angle changes, it will not be used further. A number of suggested extreme datapoints, Table 4, are included in the plots, with the geometry of the extreme *SEESAW* stereochemistry illustrated in Fig. 5. The 29 datapoints in Fig. 6 vary from trigonal bipyramidal (TBP) to near regular square-based pyramidal (RSBP) with the τ values decreasing from 0.88 to 0.06 as the Cu—N4 distances increase from 2.087 (5) to 2.345 (3) Å, respectively. The datapoints show a broad *inverse* trend and clearly do not cluster around the RTBP geometrical point. This plot provides an overview of the observed stereochemistries of the $[Cu(chelate)_2X]Y$ series of complexes. Two possible parallel pathways pass through or close to seven and nine datapoints, respectively, and two datapoints lying nearby. Three of the remaining datapoints lie

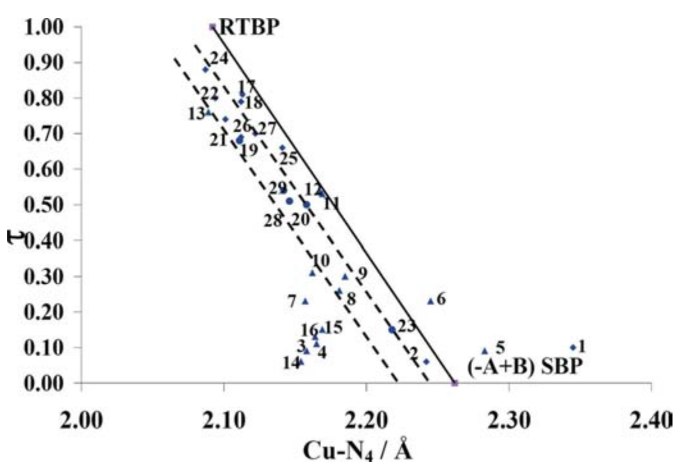

Figure 6
Plot of τ *versus* Cu—N4: ▲ dpyam, ● bipy, ◆ phen.

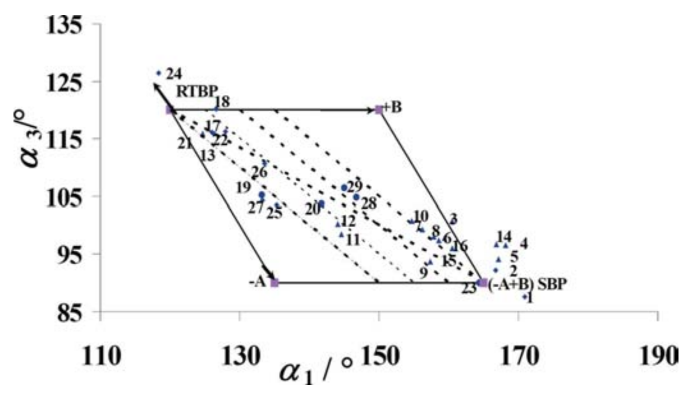

Figure 7
Plot of α_1 *versus* α_3: ▲ dpyam, ● bipy, ◆ phen.

above the RTBP → RSBP pathway and eight dpyam/pseudohalide datapoints clearly lie below the two parallel pathways, which differ significantly from the phen and bipy series in the τ values of complexes owing to the more flexible dpyam ligand. The five bipy/pseudohalide datapoints clearly overlap the phen/pseudohalide datapoints, but are shifted to slightly lower τ and higher Cu—N4 values. The highest τ value is the 0.88 datapoint, which involves the lowest τ value of 0.06 and Cu—N4 distances ranging from 2.242 to 2.087 Å. Both datapoints are in the phen/pseudohalide series. In contrast, the five bipy/pseudohalide datapoints show a much more limited range, with τ ranging from 0.80 to 0.15 and Cu—N4 distances ranging from 2.218 to 2.094 Å.

The datapoints in Fig. 7 show the α_3 values decreasing from 126.4 (1) to 87.6 (1)° as the α_1 values concomitantly increase from 118.4 (1) to 170.9 (1)°. There are 29 datapoints which have α_1 values > 120° and α_3 values < 120°, except datapoint (24) (Table 2). There are 21 datapoints found in the $-A$ $+B$ section of the graph. The exceptions are the seven datapoints (1)–(5), (14) and (24), which are in the $-A$ $+B$ section, with a small $+A$ + B (24) route sense of distortion. It is noticeable that within the α_1 and α_3 datasets, these datapoints have greater α_1 and α_3 values compared with those of the RSBP and RTBP stereochemistry. There is only one datapoint (18), which lies on the RTBP ⇒ $+B$ distortion pathway. There are also four datapoints [(17), (22), (23) and (26)], which lie on the RTBP ⇒ RSBP ($-A$ + B) distortion pathway. Four datapoints [(7), (8), (10) and (16)] and the RSBP datapoint are on the line and show an *inverse* trend, with each of these datapoints having α_2 = 105 ± 2°. The remaining datapoints, three [(9), (28) and (29)], three [(12), (20) and (21)] and one (13), lie on three possible parallel correlations (- - -) displaying α_2 values of 110 ± 2, 115 ± 1 and 120 ± 1°, respectively. This series of four possible parallel correlations have the same gradients. The datapoints show an SBP distortion, but only the correlation containing the datapoints corresponding to an α_2 value of 105° can contribute to RSBP. For each parallel correlation the α_2 values remain constant, therefore $\Delta\alpha_1\uparrow \simeq \Delta\alpha_3\downarrow$ as $\alpha_1 + \alpha_2 + \alpha_3 = 360°$, possibly suggesting the occurrence of preferred or magic angles (Murphy & Hathaway, 2003*a*,*b*; Murphy, Aljabri, Light & Hursthouse, 2004; Murphy, Roberts, Tyagi & Hathaway, 2004).

The datapoints in Fig. 8 show the Cu—N2 distances decreasing from 2.108 (1) to 2.014 (1) Å, while the Cu—N4 distances increase from 2.089 (1) to 2.345 (1) Å. There are 14 datapoints observed in the $-A$ + B quadrant of the graph, with seven points [(1), (5), (10), (13), (14), (22), (26)] lying outside this quadrant. There are six datapoints [(3), (4), (7), (21), (28), (29)] on the RTBP ⇒ $+B$ trendline, and there is one datapoint (24) which lies directly on the RTBP ⇒ $\pm A$ route pathway. There is only one datapoint (11), which also lies precisely on the RTBP ⇒ RSBP ($-A$ + B) pathway, with datapoints (2), (6) (12) and (17) lying close by.

The dataplot of $a_{2,1}$ *versus* a_3 in Fig. 9 involves $a_{2,1}$ angles ranging from 171 to 94° and a_3 angles from 127 to 87°, and indicates a general increase in the separation of a_2 and a_1 angles from high to low a_3 angles. At high a_3 angles, 127–119°, the spread in $\Delta a_{2,1}$ is small, 14°, as $a_1 + a_2 + a_3 = 360°$, but at lower a_3 angles, 116–95°, the spread increases to a maximum of 73° at 96.6° of datapoint (4) and then decreases 2.3° at a_3 angles of 93–87° [datapoint (1)]. The average $a_{2,1}$ angle of 120° at an a_3 angle of 120° increases to 138.5° ($-A$ route) at an a_3 angle of 95°, and corresponds to the effect of pure $\nu_{\rm sym}^{\rm bend}$ on the a_3 angle. Within the a_3 range 120–87°, the values of the indi-

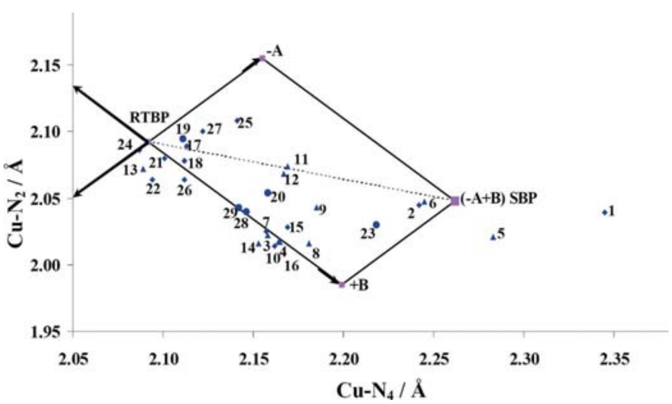

Figure 8
Plot of Cu—N2 *versus* Cu—N4: ▲ dpyam, ● bipy, ◆ phen.

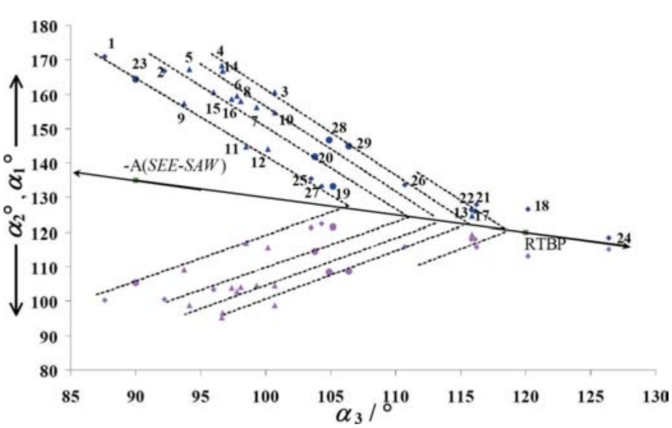

Figure 9
Plot of α_2, α_1 *versus* α_3: ▲ dpyam, ● bipy, ◆ phen.

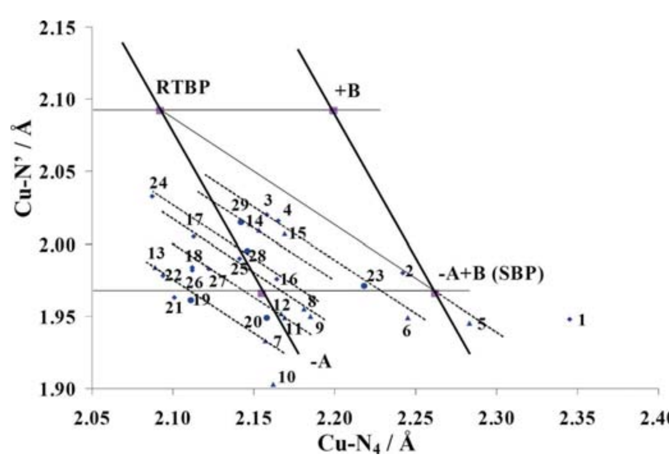

Figure 10
Plot of Cu—N′ *versus* Cu—N4: ▲ dpyam, ● bipy, ◆ phen.

vidual a_1 and a_2 angles are evenly distributed about the mean $a_{2,1}$ line. This corresponds to the effect of a pure $\nu_{\rm asym}^{\rm bend}$ mode of vibration superimposed onto the pure $\nu_{\rm sym}^{\rm bend}$ mode of vibration. The symmetric nature of the data of Fig. 9 about the RTBP $\rightarrow$ $-A$ route dataline and the restriction to the $\Delta a_{2,1}$ angle at high and low a_3 angles suggests a strong link of the $\nu_{\rm sym}^{\rm bend}$ and the $\nu_{\rm asym}^{\rm bend}$ modes of vibration. The seesaw structure ($a_1 = a_2 = 135^\circ$ and $a_3 \simeq 90^\circ$) is consistent with the formation of a pure $-A$ route distortion (Murphy, Nagle, Murphy & Hathaway, 1997; Murphy *et al.*, 1998, 2003), where the effect of $\nu_{\rm asym}^{\rm bend}$ is reduced to zero.

A feature of Fig. 9 is the formation of a number of interpenetrating right-pointing arrowhead structures, generated by reasonably linear correlations of the separate α_1 and a_2 datapoints against the a_3 datapoints. Within the arrowhead the spread in the $\Delta a_{2,1}$ angles and the range in the a_3 angles are limited to < 73 and 10°, respectively, and the tip of the arrow lies on the RTBP $\rightarrow$ $-A$ route pathway. This suggests that as a_3 decreases there is a limit to the spread in $\Delta a_{2,1}$ and the a_3 angle flips to a lower value. Thus, Fig. 9 presents a clear visual picture of the combined effect of the $\nu_{\rm sym}^{\rm bend}$ and the $\nu_{\rm asym}^{\rm bend}$ modes of vibration on the in-plane a_{1-3} angles.

The 29 datapoints in Fig. 10 range from 1.903 to 2.033 Å in the Cu—N′ distance and from 2.087 to 2.345 Å in the Cu—N4 distance, with a slight gap in the Cu—N′ datapoints from 1.97 to 2.03 Å, but not in the Cu—N4 distance. There are no datapoints lying near the RTBP datapoint, in contrast, almost all the datapoints are around the $-A$ route distortion. Correlations may be drawn in the data parallel to the RTBP $\rightarrow$ RSBP pathway, through five, four, three and two datapoints, but these are significantly displaced from the main pathway (RTBP $\rightarrow$ RSBP). This displacement is most noticeable at the lower Cu—N′ distances, suggesting that the Cu—N4 distances are more associated with the RTBP $\rightarrow$ $-A$ route pathway of the '*SEESAW*' type (IV) structure of Fig. 5. The displacement of the Cu—N4 distances to lower values can be understood in terms of a progression of the pure $n\nu_{\rm asym}^{\rm str}$ modes of vibration, giving an association of the Cu—N4 distances with the RTBP $\rightarrow$ $-A$ route distortion.

Fig. 11(*a*) shows the RTBP $\rightarrow$ $-A$ route distortion of 29 datapoints, while Fig. 11(*b*) shows the RTBP $\rightarrow$ $+B$ route distortion. Consequently, Fig. 12 has been simplified in order to qualitatively determine the directions of distortion along the $\pm A \pm B$ routes of the structural pathways.

Fig. 12 is modified from Fig. 5 in order to clearly visualize the distortion route of a given compound which is the best representation of all the datapoints in the structural pathways. The RTBP is the reference point of all routes, the other routes represent the in-plane distortion from RTBP, both in angles and distances (120, 120 and 120° for in-plane angles and 2.1, 2.1 and 2.1 Å for in-plane distances), which consider vibrational modes ($\nu_{\rm sym}^{\rm str}$, $\nu_{\rm sym}^{\rm bend}$, $\nu_{\rm asym}^{\rm str}$ and $\nu_{\rm asym}^{\rm bend}$). Thus, the standard uncertainties of angles and distances are essential in determining the magnitude of distortion for the other routes which are distorted from RTBP. The datapoints of the standard uncertainties of the distances and angles of the other routes are shown in Table 5. The standard uncertainties in SBPDTBP, RevTBP, *SEESAW* and Extreme *SEESAW* routes are only considered in angles which correspond to the pure $\nu_{\rm sym}^{\rm bend}$ in Fig.

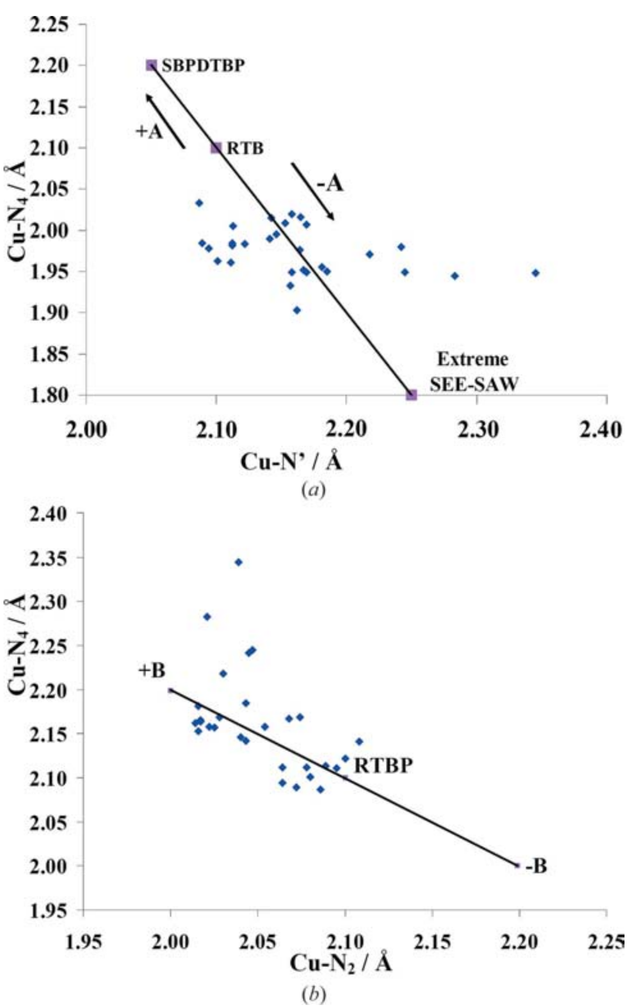

Figure 11
Plots of (*a*) Cu—N′ *versus* Cu—N4 and (*b*) Cu—N2 *versus* Cu—N4: ▲ dpyam, ● bipy, ◆ phen.

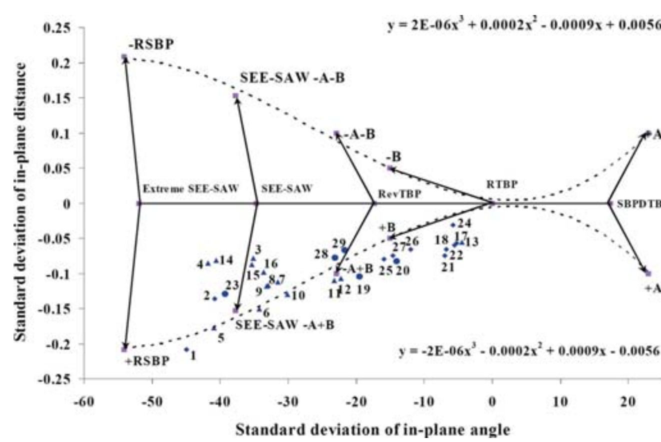

Figure 12
Plot of standard deviation of the in-plane angle *versus* standard deviation of the in-plane distance of the total data following the structural pathway shown in Fig. 3: ▲ dpyam, ● bipy, ◆ phen.

Table 5
The standard uncertainties (s.u.) in the in-plane angles and distances of other routes and sample datapoints.

S.u. in angle	S.u. in distance	
0	0	RTBP (I)
17.32051	0	SBPDTBP (II)
−17.3205	0	RevTBP (III)
−34.641	0	SEESAW (IV)
−51.9615	0	Extreme-SEESAW (V)
−15	−0.05	+*B* (VI)
22.91288	−0.1	+*A* + *B* (VII)
−22.9129	−0.1	−*A* + *B* (VIII)
−37.7492	−0.15275	SEESAW −*A* + *B* (IX)
−54.0833	−0.20817	+RSBP (X)
−15	0.05	−*B* (VI′)
22.91288	0.1	+*A* − *B* (VII′)
−22.9129	0.1	−*A* − *B* (VIII′)
−37.7492	0.15275	SEESAW −*A* − *B* (IX′)
−54.0833	0.20817	−RSBP (X′)

	(5)	(6)	(7)	(8)	(9)	(10)	(11)	(12)	(13)	(1)
S.u. in distance	−0.17732	−0.15079	−0.11259	−0.11692	−0.11835	−0.12994	−0.11034	−0.10761	−0.05636	−0.20798
S.u. in angle	−40.85743	−34.21286	−31.48243	−32.95467	−33.17971	−30.11428	−23.20582	−22.27338	−4.43058	−44.90015

	(19)	(20)	(3)	(4)	(14)	(15)	(2)	(23)	(21)	(22)
S.u. in distance	−0.08237	−0.1045	−0.0791	−0.08574	−0.08119	−0.0881	−0.13643	−0.12899	−0.07436	−0.06021
S.u. in angle	−14.06840	−19.53945	−35.08689	−41.74829	−40.53011	−35.29736	−40.80445	−39.27153	−6.93109	−5.55608

	(16)	(17)	(18)	(24)	(25)	(26)	(27)	(28)	(29)
S.u. in distance	−0.09886	−0.05671	−0.0663	−0.03089	−0.07939	−0.06574	−0.07472	−0.07753	−0.06673
S.u. in angle	−33.61493	−5.25389	−6.70224	−5.76888	−15.93393	−12.04035	−14.64821	−23.16405	−21.67856

5. For the remaining routes, the standard deviations are considered in both distances and angles. The polynomial fitting curves are displayed in the equations presented in Fig. 12. There are 29 sample datapoints in Fig. 12 which show distortion from RTBP to −*A* + *B* and continue to +RSBP. There is not even one datapoint distorted from RTBP to +*A* and/or −*B*. This is explained as the inherent feature of five-coordinate copper(II) complexes with a pseudohalide ligand system. In this system most datapoints lie below and above the polynomial curve, but are spread over a wide range of distortions from RTBP → RSBP. Datapoint (1) is distorted to near +RSBP, which is the most distorted from RTBP found so far for this family of complexes. Most of the datapoints of phen/pseudohalide lie below the polynomial curve and are distorted from RTBP to –*A* + *B*. Only datapoint (2) lies above the polynomial curve and is found to be distorted from *SEESAW* −*A* + *B* to +RSBP. Thus, (1) and (2) show extremely distorted stereochemistries, which is unusual for the phen analogue as most of the phen/pseudohalide are usually found in RTBP → −*A* + *B*. Additionally, complex (1) has a Cu—N4 distance of 2.345 Å, which is the longest Cu—N distance for a phen chelate attached to Cu. The datapoints of the dpyam/pseudohalide point towards −*A* + *B* to +RSBP owing to the more flexible dpyam ligand; only datapoint (13) (τ = 0.76) points to RTBP → +*B* which equates to an unusual SBPDTBP stereochemistry for dpyam/pseudohalide. The datapoints of bipy/pseudohalide are usually found in RTBP → −*A* + *B*; only datapoint (23) shows the distortion from *SEESAW* −*A* + *B* to +RSBP.

3.5. General conclusions from the [Cu(chelate)$_2X$]Y series scatterplot data

The information obtained from the scatterplot analysis of this series of 29 [Cu(chelate)$_2X$]Y complexes with a pseudohalide ligand can be summarized as follows:

(i) The data refer to a total of 29 chelate/pseudohalide single-crystal structures of the [Cu(chelate)$_2X$]$^+$ cation distortion isomers, where X = NCO (12 complexes), N_3 (six complexes), NCS (five complexes) and C_2N_3 (six complexes), in lattices of different Y^- anions.

(ii) The stereochemistry of the phen/pseudohalide series has τ values in the range 0.88–0.06, while those of the bipy/pseudohalide series are in the range 0.80–0.15 and those of the dpyam/pseudohalide series appear in the range 0.76–0.09. However, the dpyam/pseudohalide series of complexes show a clear difference from the phen and bipy series that most τ values appear in the range 0.09–0.54, while those of the bipy, phen/pseudohalide are found in the range 0.88–0.51 owing to the more flexible dpyam ligand. The phen complex (2) has a τ value of 0.06, which indicates the most RSBP found so far in a series of five-coordinate copper(II) complexes with a pseudohalide ligand.

Table 6
Electronic reflectance data for [Cu(dpyam)$_2X$]Y complexes.

Complex	τ	Peak energy (10^3 cm^{-1})
(3)	0.09	14.49, 10.17
(4)	0.11	14.45, 10.42
(5)	0.09	14.51, 10.15
(6)	0.23	14.42, 10.18
(7)	0.23	14.24, 10.22
(8)	0.26	14.20, 10.35
(9)	0.30	13.93, 10.27
(10)	0.31	14.23, 10.63
(11)	0.53	13.87, 10.33
(12)	0.54	13.80, 10.35
(13)	0.76	12.88, 11.42
(14)	0.06	14.05, 11.01
(15)	0.15	14.00, 11.11
(16)	0.13	15.74, 10.66
RTBP	1.00	12.00

(iii) Of the 29 datapoints, three lie above the RTBP–RSBP line and eight lie below the RTBP–RSBP line in Fig. 6, in a random distribution. For the remaining 18 datapoints, the distribution is not random and there is clear evidence of linear pathways (Bersuker, 2001), significantly parallel to the RTBP $\rightarrow$ RSBP ($-A$ + B) route distortions associated with the structural pathways of Fig. 5.

(iv) Within the two scatterplots of Figs. 7 and 10, significant parallel correlations are observed. Most of the datapoints are in the range $-A + B$ and the correlation can be understood in terms of coupling into linear progressions (Nakamoto, 1978) the four in-plane modes of vibration of the CuN$_4$N$'$ chromophore (Bacci, 1986; Holmes *et al.*, 1969), all of which are of A symmetry (Reinen, 1983; Reinen & Atanasov, 1991) in the C_1 point group (Fig. 5).

(v) Within the scatterplot of Fig. 9, there is clear evidence for a right-pointing arrowhead structure which has limited ranges of a_3 angles. The 'flips' to adjacent arrowheads are associated with progressions in the pure $n\nu_{\rm sym}^{\rm bend}$ modes of vibration and are related to the individual parallel pathways of Fig. 7.

(vi) Together the scatterplots of Figs. 6–10 present the most convincing evidence for the involvement of the four in-plane modes of vibration of the CuN$_4$N$'$ chromophore (Fig. 2) in determining the direction of the distortion along the $\pm A$ $\pm B$ routes of the structural pathways of Fig. 5.

(vii) The best scatterplot (Fig. 12) is introduced to determine the directions and magnitude of distortion in the structural pathways, compared with the results from Figs. 7 and 10 which involve the distortion from RTBP $\rightarrow$ $-A$ + B route.

(viii) The present structural pathway (Fig. 5) is modified from the previously reported pathway (Youngme, Phatchimkun, Suksangpanya *et al.*, 2007). The extended routes are Extreme *SEESAW*, +RSBP and −RSBP, in order to explore the distortion of all the datapoints available for the dpyam, phen and bipy/pseudohalides series.

(ix) A new modification has been made to the N1—Cu—N3 angle (α_8) in order to obtain τ = 0 for RSBP (Fig. 5).

3.6. IR and electronic properties of the [Cu(chelate)$_2X$]Y complexes

The IR spectra display a strong band at 2213 cm^{-1} for (1), 2221 cm^{-1} for (2), which can be assigned to the $\nu_{\rm asym}$(NCO) absorption band, and a strong band at 2042 cm^{-1} for (3) and 2038 cm^{-1} for (4), which can be assigned to the $\nu_{\rm asym}$(N$_3$) absorption band. The spectrum of (3) displays intense bands at approximately 1384 and 1323 cm^{-1}, consistent with the characteristic peaks of $\nu_{\rm as}$(NO) and $\nu_{\rm s}$(NO) of the NO_3^- anion. The spectrum of (4) displays a broad and intense band at approximately 1106–1060 cm^{-1}, consistent with the characteristic peak of the ClO_4^- anion.

The polycrystalline electronic reflectance spectra of some representative complexes are shown in Table 6 (Harrison *et al.*, 1981; Nagle *et al.*, 1990) as illustrated examples. Complexes (1)–(4), τ = 0.10, 0.06, 0.09 and 0.11, which have a TBDSBP stereochemistry, involve a high-energy, high-intensity peak at 13 570 cm^{-1} for (1), 14 400 cm^{-1} for (2), 14 490 cm^{-1} for (3) and 14 450 cm^{-1} for (4), with a low-energy, low-intensity shoulder at 11 140 cm^{-1} for (1), 10 110 cm^{-1} for (2), 10 170 cm^{-1} for (3) and 10 420 cm^{-1} for (4). The one-electron ground-state configuration is $d_{x^2-y^2} > d_{z^2} > d_{xy} > d_{xz} \simeq d_{yz}$, and the transitions may be assigned as the $d_{z^2} \Rightarrow d_{x^2-y^2}$ transition

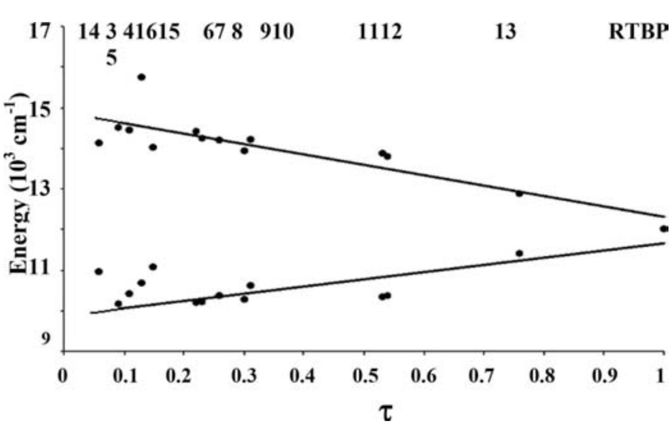

Figure 13
Plot of τ value *versus* electronic energies for [Cu(dpyam)$_2X$]Y complexes.

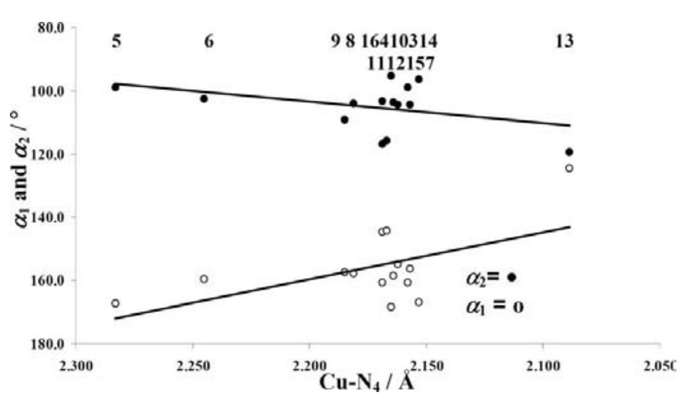

Figure 14
Plot of the two basal angles α_1 and α_2 *versus* the Cu—N4 values for [Cu(dpyam)$_2X$]Y.

for the low-energy shoulder and the $d_{xz} \simeq d_{yz} \Rightarrow d_{x^2-y^2}$ transition for the high-energy peak.

The corresponding spectro-structural correlation plots (Fig. 13) reveal that ΔE values increase with increasing τ values for the low-energy peak and the reverse result has been found for the higher-energy peak. It is evident from Fig. 14 that the basal angles themselves have a similar trend to the ΔE values. This plot clearly indicates that a linear correlation between τ and the ΔE values exists in (3)–(16).

The authors gratefully acknowledge the Thailand Research Fund (Grant Numbers: RTA 4880008 and BRG 4980007), Khon Kaen University and the Center for Innovation in Chemistry: Postgraduate Education and Research Program in Chemistry (PERCH-CIC), Thailand, for financial support.

References

Addison, A. W., Rao, T. N., Reedijk, J., Rijn, van J. & Verschoor, G. C. (1984). *J. Chem. Soc. Dalton Trans.* pp. 1349–1356.

Addison, A. W., Rao, T. N. & Sinn, E. (1984). *Inorg. Chem.* **23**, 1957–1967.

Akhter, P. & Hathaway, B. (1991). *Acta Cryst.* C**47**, 86–89.

Bacci, M. (1986). *J. Chem. Phys.* **104**, 191–199.

Bersuker, I. B. (2001). *Chem. Rev.* pp. 1067–1114.

Bruker (2000). *SHELXTL*, Version 6.12. Bruker AXS Inc., Madison, Wisconsin, USA.

Bruker (2001*a*). *SAINT*, Version 6.02. Bruker AXS Inc., Madison, Wisconsin, USA.

Bruker (2001*b*). *SMART*, Version 5.054. Bruker AXS Inc., Madison, Wisconsin, USA.

Burčák, M., Potočňák, I., Baran, P. & Jäger, L. (2004). *Acta Cryst.* C**60**, m601–m604.

Burgi, H. & Dunitz, J. D. (1983). *Acc. Chem. Res.* **16**, 153–161.

Camus, A., Facchinetti, A., Marsich, N., Lanfredi, A. M. M. & Ugozzoli, F. (1999). *Inorg. Chim. Acta*, **290**, 180–188.

Dunitz, J. D. (1979). *X-ray Analysis and Structure of Organic Molecules*, ch. 7. London: Cornell University Press.

Gazo, J., Bersuker, I. B., Garaj, J., Kabešová, M., Kohout, J., Langfelderová, H., Melnik, M., Serator, M. & Valach, F. (1976). *Coord. Chem. Rev.* **19**, 253–297.

Harrison, W. D., Kennedy, D. M., Ray, N. J., Sheahan, R. & Hathaway, B. J. (1981). *J. Chem. Soc. Dalton Trans.* pp. 1556–1564.

Hathaway, B. J. (1984). *Struct. Bonding (Berlin)*, **57**, 55–118.

Hathaway, B. J. & Billing, D. E. (1970). *Coord. Chem. Rev.* **5**, 143–207.

Holmes, R. R., Deiters, R. S. & Golen, J. A. (1969). *Inorg. Chem.* **8**, 2612–2620.

Huq, F. & Shapski, A. C. (1971). *J. Chem. Soc. A*, p. 1927.

Jahn, H. A. & Teller, E. (1937). *Proc. R. Soc. London*, **161**, 220–235.

Jensen, W. P. & Jacobson, R. A. (1981). *Inorg. Chim. Acta*, **49**, 199–204.

Johnson, J. E. & Jacobson, R. A. (1973). *J. Chem. Soc. Dalton Trans.* pp. 580–584.

McAuliffe, C. A., Pritchard, R. G., Bermejo, M. R., Garcia-Vazquez, A., Macias, A., Sanmartín, J., Romero, J. & Sousa, A. (1992). *Acta Cryst.* C**48**, 1316–1317.

Munno, G. D., Lombardi, M. G., Julve, M., Lloret, F. & Faus, J. (1998). *Inorg. Chim. Acta*, **282**, 82–89.

Murphy, B., Aljabri, M., Light, M. & Hursthouse, M. B. (2003). *J. Chem. Cryst.* **33**, 195–202.

Murphy, B., Aljabri, M., Light, M. & Hursthouse, M. B. (2004). *Transition Met. Chem.* **29**, 394–399.

Murphy, B. & Hathaway, B. J. (2003*a*). *Coord. Chem. Rev.* **243**, 237–262.

Murphy, B. & Hathaway, B. J. (2003*b*). *J. Coord. Chem.* **56**, 493–510.

Murphy, B., Roberts, G., Tyagi, S. & Hathaway, B. J. (2004). *J. Mol. Struct.* **698**, 25–36.

Murphy, G., Nagle, P., Murphy, B. & Hathaway, B. J. (1997). *J. Chem. Soc. Dalton Trans.* pp. 2645–2652.

Murphy, G., O'Sullivan, C., Murphy, B. & Hathaway, B. J. (1998). *Inorg. Chem.* **37**, 240–248.

Nagle, P., O'Sullivan, E., Hathaway, B. J. & Muller, E. J. (1990). *J. Chem. Soc. Dalton Trans.* pp. 3399–3406.

Nakamoto, K. (1978). *Infrared Spectra of Inorganic and Coordination Compounds*, 3rd ed. New York: Wiley.

Parker, O. J., Manson, J. L. & Breneman, G. L. (1994). *Acta Cryst.* C**50**, 1201–1203.

Potočňák, I., Burcák, M., Baran, P. & Jäger, L. (2005). *Trans. Met. Chem.* **30**, 889–896.

Potočňák, I., Burčák, M., Massa, W. & Jäger, L. (2002). *Acta Cryst.* C**58**, m523–m528.

Potočňák, I., Burčák, M., Wagner, C. & Jäger, L. (2003). *Acta Cryst.* C**59**, m252–m254.

Potočňák, I., Dunaj-Jurčo, M., Mikloš, D. & Jäger, L. (1996*a*). *Acta Cryst.* C**52**, 1653–1655.

Potočňák, I., Dunaj-Jurčo, M., Mikloš, D. & Jäger, L. (1996*b*). *Acta Cryst.* C**52**, 532–535.

Potočňák, I., Dunaj-Jurčo, M., Mikloš, D. & Jäger, L. (1998*a*). *Acta Cryst.* C**54**, 313–315.

Potočňák, I., Dunaj-Jurčo, M., Mikloš, D. & Jäger, L. (1998*b*). *Acta Cryst.* C**54**, 1760–1763.

Potočňák, I., Dunaj-Jurčo, M., Mikloš, D., Kabešová, M. & Jäger, L. (1995). *Acta Cryst.* C**51**, 1291–1293.

Potočňák, I., Dunaj-Jurčo, M., Mikloš, D., Massa, W. & Jäger, L. (2001). *Acta Cryst.* C**57**, 363–365.

Reinen, D. (1983). *Comments Inorg. Chem.* **2**, 227–246.

Reinen, D. & Atanasov, M. (1991). *Magn. Reson. Rev.* **15**, 167–239.

Reinen, D. & Friebel, C. (1984). *Inorg. Chem.* **23**, 791–798.

Sheldrick, G. M. (1996). *SADABS*. University of Göttingen, Germany.

Sheldrick, G. M. (2008). *Acta Cryst.* A**64**, 112–122.

Siemens (1996). *SAINT*. Siemens Analytical X-ray Systems Inc., Madison, Wisconsin, USA.

Siemens (1997). *SHELXTL*, Version 6.12. Siemens Analytical X-ray Systems, Inc., Madison, Wisconsin, USA.

Youngme, S., Chaichit, N., Pakawatchai, C. & Booncoon, S. (2002). *Polyhedron*, **21**, 1279–1288.

Youngme, S., Phatchimkun, J., Pakawatchai, C., Prabpai, S. & Kongsaeree, P. (2007). *Acta Cryst.* C**63**, m45–m47.

Youngme, S., Phatchimkun, J., Suksangpanya, U., Pakawatchai, C., Chaichit, N., Kongsaeree, P., Krzystek, J. & Murphy, B. (2007). *Polyhedron*, **26**, 871–882.